Journal of Structural Geology, Vol. 11, No. 1/2, pp. 175 to 189, 1989
Printed in Great Britain

0191-8141/89 $03.00 + 0.00

Development of shape and lattice preferred orientations: application to the seismic anisotropy of the lower crust

DAVID MAINPRICE and ADOLPHE NICOLAS

Laboratoire de Tectonophysique, Place E.Bataillon, 34060 Montpellier Cédex, France

(*Received* 23 *May* 1988; *accepted* 20 *October* 1988)

Abstract—We review the physical basis of the development of fabrics in plastic and viscous flow and illustrate the typical fabrics formed by these processes in the main rock-forming silicates of the lower crust (feldspar, quartz, pyroxene and amphibole). The orientation process in plastic deformation where a single slip is dominant is recalled and the role of the constraint of neighbouring grains is emphasized. The fabric development of anisometric crystals in viscous flow is discussed as a function of the main controlling parameters: shear strain, aspect ratio and interference between crystals. The same sense of fabric asymmetry is introduced by plastic and viscous flow between the flow plane and the shape preferred orientation and hence coherent kinematic analysis can be undertaken in both modes of flow.

In order to assess the role of such fabrics in the seismic laminations of the lower continental crust we have calculated the seismic P-wave properties of typical fabrics for hypothetical monomineralic and polymineralic rocks. The calculations show that the strongest anisotropies develop in monomineralic rocks with values between 5 and 16%, compared with 5 and 8% for typical rock compositions. The strongest anisotropies for layered monomineralic rocks generated by fabrics is only 6% compared to the 14% suggested by model studies of the observed seismic laminations. We suggest that other effects, such as compositional layering and/or constructive interference of seismic waves are responsible for augmenting the apparent anisotropy.

INTRODUCTION

OVER the last 15 years important progress has been made in the interpretation of lattice preferred orientation (LPO) (see reviews by Bunge 1982, Wenk 1985, Nicolas 1987) in rocks plastically deformed by large homogenous flow. Understanding the development of these fabrics has allowed geologists to go beyond geometrical or structural analyses and undertake kinematic analyses (Nicolas *et al.* 1972). In view of new perspectives for the application of fabrics, like those presented below, we wish in this paper to review the general subject of fabrics in plastic flow and to introduce new results for the case of rocks deformed by a large magmatic flow.

The recent interest in the lower crust has been stimulated by deep crustal seismic and deep borehole projects in various countries. The interpretation of these new data requires a closer liaison between structural geologists and geophysicists, and a better understanding of the relationship between the acquisition of anisotropic properties and their geophysical expression. We assess the importance of fabric studies to the seismic character of the lower crust, first by reviewing the typical fabrics of the volumetrically important silicate minerals, and secondly, by calculating the P-wave anisotropy of monomineralic and polymineralic rocks from their typical fabric patterns.

A simplified mechanical picture of a continental crust–upper mantle of the Earth is shown in Fig. 1(a). We stress that the picture is schematic, as variations in thermal gradient, compositional stratification, strain rate (and hence deformation mechanism) and fluid pressure may drastically change the local picture. The strength as a function of depth helps to emphasize the major mechanical divisions; an upper crust in which brittle fracture is dominant and a lower crust in which plastic flow is dominant. The strength increases with depth and confining pressure in the upper crust as it becomes increasingly difficult to open new cracks or slide along old ones. The strength decreases with depth and increasing temperature in the lower crust as thermally activated processes, such as diffusion-controlled dislocation climb, accelerate the plastic processes. An important mechanical boundary occurs between our

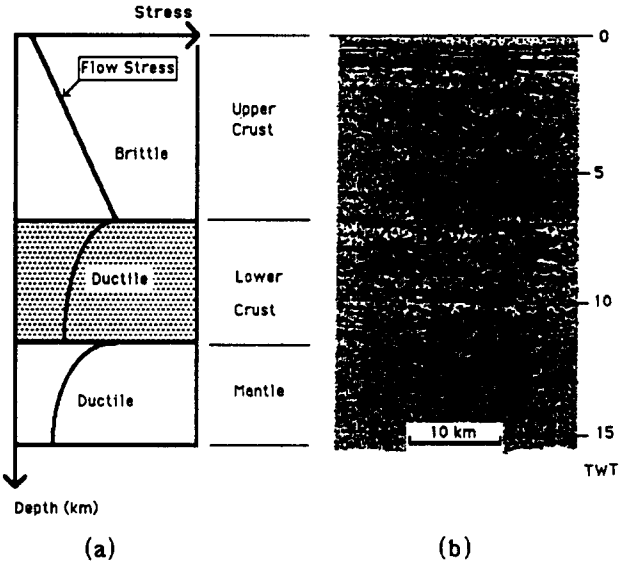

Fig. 1. Schematic mechanical sub-divisions of the crust (a) and their correlation with the seismic profile (b). The brittle upper crust is seismically transparent, and the ductile lower crust is seismically reflective. The flow stress in (a) for a constant strain rate is shown as a solid line. TWT = two way travel time in seconds.

mechanically defined upper and lower crust, that is the brittle–ductile transition. It has been proposed that this important transition is the locking point for active faults (Sibson 1979).

In the lower crust there is a gradual increase in mafic content with depth. At the lower crust–mantle boundary an important mechanical discontinuity occurs between the chemically felsic crustal rocks and the ultramafic mantle rocks. Kirby (1985) has suggested that this rheological discontinuity occurs at the Moho due to the larger temperature sensitivity (as expressed by the apparent activation energy) for plastic flow of mantle rocks.

THE ORIGIN OF PREFERRED ORIENTATION

LPO in minerals can be produced by several physically distinct processes: for example plastic flow with or without recrystallization, viscous flow and anisotropic crystal growth. In what follows we will limit ourselves to a discussion of the important mechanisms in large-scale ductile plastic and viscous deformation and will not consider the growth process.

Plastic flow

It is now well established both by experimental and natural studies, that plastic flow induces preferred orientations in minerals (see review by Nicolas & Poirier 1976). The respective roles of deviatoric stress and plastic strain in the development of preferred orientations have long been debated and in view of the consequences for seismic anisotropy this necessitates a brief summary of the fundamental physical mechanisms.

In the plastic field, crystals deform principally by dislocation slip. The contribution of deformation mechanisms controlled by diffusion (dislocation climb, grain-boundary sliding), which may be important at high temperature when diffusion becomes efficient, is overlooked in this discussion as they do not contribute directly to the development of preferred orientations.

To assume continuity of a deforming crystal with its neighbours during the course of an arbitrary deformation, five independent directions of motion are necessary. This can be achieved in a crystal by the activation of five independent slip systems (the von Mises criterion) or with a combination of less slip systems and other modes of deformation: for example, diffusion, heterogeneous deformation with or without lattice rotation and fracturing. In low symmetry silicates of the lower crust, such as plagioclase, pyroxene, olivine and amphibole, five independent slip systems are not available or rarely activated. Hence we cannot use the Taylor model (e.g. Lister *et al.* 1978, Wagner *et al.* 1982) which requires five independent slip systems to explain the fabrics in these minerals. Furthermore, it is clear that such modelling schemes do not always reproduce the LPOs observed in experiments and nature, particularly the asymmetry in non-coaxial deformation (see Bouchez *et al.* 1983, Etchecopar & Vasseur 1987). New developments of this model which require less slip systems (relaxed Taylor model, Van Houette & Wagner 1985) or include physically justified recrystallization schemes may provide a better insight into fabric development (Jessell 1988).

Predominance of one slip system in certain cases is demonstrated by the analysis of dislocation microstructures resulting from experimental and natural deformation. This is also suggested by petrofabric diagrams where point maxima, related to the structural frame, are commonly populated by crystal axes coinciding with easy slip directions or poles of easy slip planes. In contrast, more complex diagrams are obtained in minerals where several slip systems operate simultaneously, such as in the high-temperature deformation of calcite with the activation of twinning and two slip planes. As a result, the relation between the slip systems and the structural frame is complex (Wagner *et al.* 1982, Wenk *et al.* 1987).

For these reasons the following kinematic analysis deals mainly with mineral aggregates where a single slip system is dominant. The interpretation of plastically deformed structures derives from studies in peridotites (Nicolas *et al.* 1972). The analysis has been verified in a non-coaxial deformation regime, which is the most instructive one, both in controlled experiments (Bouchez & Duval 1982) and in well characterized natural shear zones (e.g. Prinzhofer & Nicolas 1980). It can be stated as follows.

(1) In the statistically homogeneous deformation of a specimen composed of minerals characterized by a dominant slip system, the preferred orientation of slip planes and slip directions in these minerals tend to coincide with, respectively, the flow plane and the flow line.

(2) The flow regime can be deduced from the relative (preferred) orientation of the slip systems and the finite-strain directions (X,Y,Z). An asymmetry of the slip directions and slip planes with respect to X,Y,Z is taken as an indication of non-coaxial deformation and provides a means by which to deduce the shear sense.

Figure 2(a) illustrates the deformation of a crystal by a single slip system correctly oriented with respect to the applied shear stress. The rules consist in extending to the aggregate the behaviour of this individual Fig. 2(b).

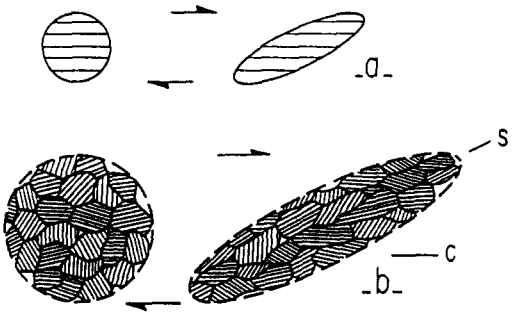

Fig. 2. Relationship between (S) shape, (L) lattice fabric and shear plane (C). (a) Single crystal with a slip plane appropriately orientated. (b) Aggregate with a dominant slip system, shaded lines representing the slip planes.

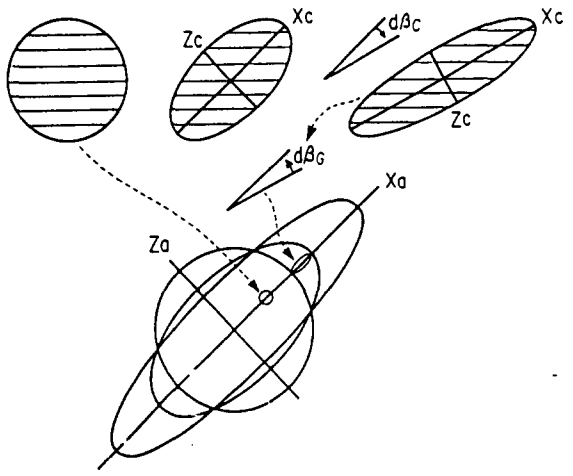

Fig. 3. Lattice reorientation in a crystal with a single slip system during progressive pure shear deformation of the enclosing aggregate. See text for explanation.

With increasing strain, the crystals will progressively be reoriented to mimic the single crystal behaviour. Let us examine how this reorientation proceeds in two dimensions, with single slip.

Simple shear in a crystal rotates all the lines attached to the crystal except those which are contained in the slip plane (Fig. 2a). Let us suppose that the deforming crystal illustrated by Fig. 3 is embedded into an aggregate deforming by pure shear. In the aggregate, the principal finite-strain axes X_a and Z_a remain parallel during the course of deformation and impose this constraint on the crystal strain axes X_c and Z_c ($X_c \geq Y_c \geq Z_c$). Accordingly, for each $d\beta$ strain increment producing a $d\beta_C$ clockwise rotation due to shear, the X_c, Z_c axes must rotate by a back rotation of $d\beta_G$ anticlockwise angle equal to $d\beta_C$; for a given finite strain we have $\beta_C = -\beta_G$. The bulk rotation produces a lattice reorientation which in the present case would lead to a statistical preferred orientation of the slip planes close to X_a for the aggregate.

The following conclusions can be derived:

(1) The cause of lattice reorientation in a crystal is the requirement to maintain continuity with its immediate neighbours. Just as neighbours deform in approximately similar fashion to the aggregate, so must the individual crystal. Note, however, that in cases where several slip systems are active, crystals may deform in a different manner from the aggregate (for example quartzite, Law 1987).

(2) The crystal reorientations are not a direct consequence of the stress applied to the aggregate, but a response to the boundary conditions imposed by its neighbours. At the crystal scale, reorientation obeys local dynamic considerations due to the boundary conditions.

(3) With homogeneous strain and single slip in crystals, it is theoretically impossible to achieve continuity from one deforming crystal to the next (e.g. Etchecopar & Vasseur 1987). This problem is solved differently in low- and high-temperature deformations: localized lattice bending, cleavage, fracturing, kinking and recrystallization at low temperature, and more homogenous diffusion controlled precesses such as dislocation climb and grain-boundary migration at high temperature.

Viscous flow

The viscous flow of rocks containing a melt fraction above some critical value, experimentally estimated to be between 35 and 45% volume (Ariz 1978, Van der Molen & Paterson 1979), results in the shape preferred orientations (SPO) of minerals with unequal dimensions. The SPO develops because the minerals with an inequant shape are free to rotate with an angular velocity which is directly related to the macroscopic strain rate of the surrounding matrix and to their aspect ratio. For many minerals (e.g. mica, amphibole, pyroxene, olivine and feldspar), crystal growth rates are anisotropic, so crystals develop with inequant shapes which are directly related to crystallographic forms. For example, plagioclase often develops as lath-shaped crystals with prominent (010) and (001) forms elongate along the [100] direction, with typical aspect ratios (n = length/width) between 2 and 4. Hence the development of SPO in viscous deformation entails the development of LPO as there is a direct relationship between crystal shape and the crystal structure.

The theory of particle motion in a viscous flowing matrix is based on two physically distinct cases, a deformable particle (or marker) with the same mechanical properties as the matrix (March 1932) and a rigid (undeformable) particle (Jeffery 1922, Willis 1977). Real geological situations may encompass these two extremes. In the case of rigid particles, the torques exerted by the deforming matrix cause them to rotate at a velocity which is dependent on their axial ratio. The particles with larger axial ratios rotate more slowly towards the flow plane (Fernandez *et al.* 1983) (Fig. 4).

We analyse first the case of viscous flow imposed on free rigid particles (no physical contact between particles) of identical aspect ratio. If flow is coaxial, a stable orientation is attained when the long axis of particles are parallel to the long axis of the finite-strain ellipsoid. However, in non-coaxial flow such as simple shear, particles rotate indefinitely, although they tend to be

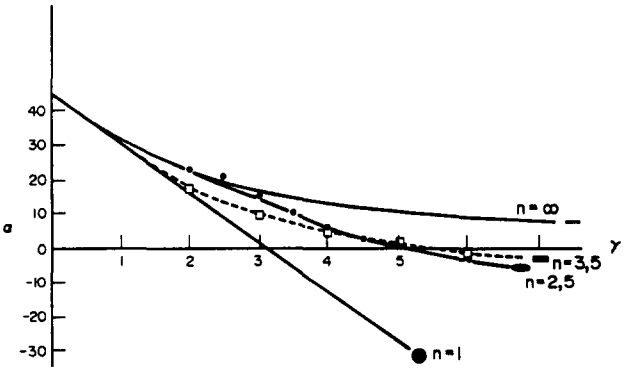

Fig. 4. Two-dimensional experimental results for simple shear from Fernandez *et al.* (1983). Angle (α) between shape fabric major axis and shear plane as a function of shear strain (γ) for markers with axial ratios n = 2.5 (black dots) and n = 3.5 (hollow squares). The theoretical limiting curves for n = 1 and $n = \infty$ are shown for reference.

statistically orientated parallel to the flow plane because this is a metastable orientation where the velocity is temporarily zero. The particles with larger axial ratios tend to stay close to the flow plane for longer periods as the torque exerted on them is very small in this orientation. In this manner a statistical planar and linear fabric is developed in which rod-like particles define a lineation and plate-like particles define a foliation. The theory has several important geological applications such as estimation of finite strain and analysis of flow regime (coaxial or non-coaxial). The March model has been successfully applied to determine the strains from preferred orientations in experimentally and naturally deformed mica aggregates (e.g. Means & Paterson 1966, Oertel 1970). Flow regimes have been investigated by Bouchez *et al.* (1981), Blumenfeld & Bouchez (1988) and Benn & Allard (in press).

Analysis of shear sense in shear flow

A monoclinic symmetry, expressed by a typical asymmetry between the trace of the shape fabric (*S*) and the flow plane (*C*), appears if any of the restrictions adopted above are relaxed (Benn & Allard in press). Interestingly, for a given sense of shear flow the obliquity is the same in the different cases and is the same as in the analysis of plastic flow. Some general rules are proposed below.

(i) A shear strain, γ, of < 4 is insufficient to rotate particles of common aspect ratios into parallelism with the flow plane (see Fig. 4). If the orientation of the flow plane (*C*) is known independently, the shear sense is deduced from its obliquity with the trace of the foliation (*S*, Fig. 5a). If there are passive markers, these record the direction of finite strain, which with increasing strain rapidly lags behind the SPO of the rigid markers, thus providing a shear-sense criterion (Fig. 5b).

(ii) For two or more sets of particles with different aspect ratios, the shear sense is deduced from the skewness of the total fabric (Figs. 5c and 6b).

(iii) Particles which cannot rotate freely, but interfere, produce an interaction called the 'tiling' effect (Fig. 5d).

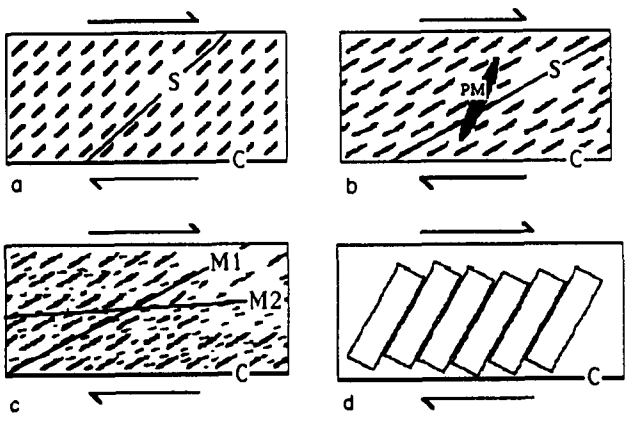

Fig. 5. Obliquity of viscous flow structures in shear deformation. (a) Shape fabric (*S*) and shear plane (*C*) (horizontal); (b) passive marker (PM ellipse) and rigid markers (lines); (c) two sets of markers (M1, M2) with different aspect ratios; (d) tiling of crystals and shear plane (*C*) (horizontal).

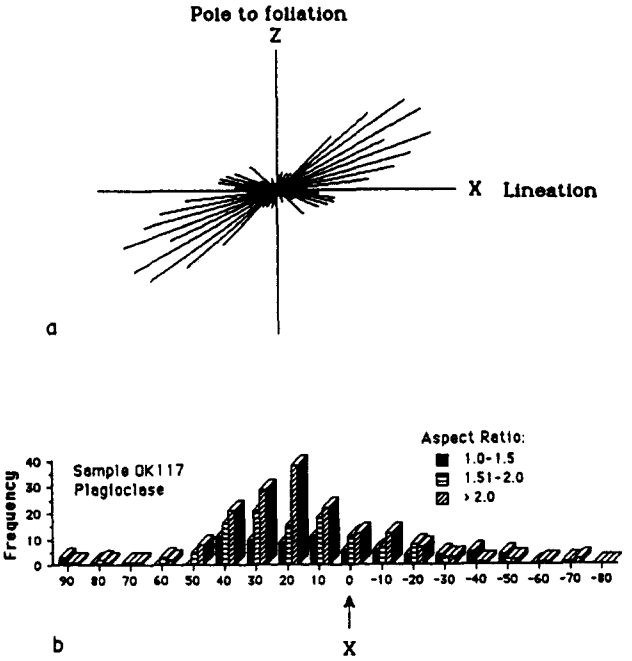

Fig. 6. SPO fabrics of plagioclase from a deformed gabbro (Benn & Allard in press). (a) Rose diagram of grain loss axis orientations in the *XZ* plane relative to the compositional layering. *N* = number of measurements, I = eigen value of best axis. (b) Bar graph of grain orientations in the *XZ* plane divided into classes according to aspect ratio. Note the maximum frequency of the largest aspect ratios is closest to the foliation.

A non-coaxial flow regime is thus characterized by a SPO which is oblique to the shear plane (*C*), and the orientation of the SPOs for different aspect ratios have different orientations (Fig. 5c). Illustration of these rules to determine the shear sense are found, for example, in the study of a viscously deformed gabbro by Benn & Allard (in press). The orientation of plagioclase grains is oblique to the compositional layering (the inferred shear plane, *C*) (Fig. 6a) and plagioclase grains with different aspect ratios have different orientations (Fig. 6b). The obliquity between SPO sub-populations with different aspect ratios have been analyzed by Fernandez *et al.* (1983) (Fig. 4) in a viscously deformed granite; these sub-populations rotate at different rates with respect to the finite-strain axes. The tiling of crystals, first invoked by Den Tex (1969) to account for the oblique fabric of olivine crystals in ultramafic rocks, has been applied by Blumenfeld (1983) to granitic intrusions. In *XZ* sections the rotation of individual crystals results in the tiling or book-shelf feature, sloping to the left (due to sinistral rotation) or to the right (dextral rotation). Statistical counting of such features or analysis of the monoclinic fabrics they induced (Benn & Allard in press) reveal the dominant sense of shear (Blumenfeld & Bouchez 1988). The obliquity of the SPO foliation (*S*) and shear plane (*C*) was also used by Blumenfeld & Bouchez in their study of a deformed granite.

Studies of LPO in viscously deformed igneous bodies demonstrate that strong preferred orientations can develop in this way. Fabrics of plagioclase from tonalite (Duffield 1968), granite (Bouchez *et al.* 1981), gabbro (Benn & Allard in press) and anorthosite (Munch 1988)

all have strong fabrics with (010) in the foliation plane. Similarly pyroxene fabrics from ultramafics (Jackson 1961), gabbro (Benn & Allard in press), wehrlite (Jackson *et al.* 1975) and pyroxenite (Jackson *et al.* 1975) with (010) in the foliation plane have been reported.

Description and analysis of LPO

Once measurements of the LPO have been completed, either by diffraction techniques (X-ray, neutron or electron diffraction) or by traditional optical microscopy, the data can be presented in the form of pole figures, inverse pole figures or sections of the orientation distribution function (ODF). In what follows we shall concentrate on the case of optical data (see Bunge 1982 for references on the treatment of diffraction data). The position of the individual crystal is recorded on the enlarged photograph of the thin section and its microstructural type (ribbon, globular, retort, recrystallized, etc.) noted on a data sheet together with the reading of the universal stage. From the universal-stage reading, the orientation of three right-handed ortho-normal reference directions (X_c, Y_c, Z_c) in each individual crystal can be recorded.

The relation between the crystal axes X_c, Y_c, Z_c and three right-handed ortho-normal specimen axes X_s, Y_s, Z_s (e.g. X_s = lineation, Z_s = pole to foliation) is conveniently described by three Euler angles psi1, phi, psi2 (Bunge 1982) which describe the rotation which brings the two co-ordinate systems into coincidence. The complete orientation of an individual crystal is described by the three Euler angles and its position in the ODF (a rectangular space with the axes $\psi 1$, ϕ, $\psi 2$). Although pole figures and inverse pole figures provide a powerful means to describe and analyse the LPO, one can only see the orientation of one axis of an individual crystal and no information is given about the orientation of the other axes. The advantage of projecting the data as points in the ODF is that the orientation of the three crystal axes (X_c, Y_c, Z_c) can be illustrated simultaneously. For example, if a high density of orientations is noted in the ODF with Euler angles psi1, phi, psi2, then the orientation of the 'favoured' orientation can be plotted on a conventional stereogram and its significance analysed.

As examples of this approach we take a typical quartz fabric from the work of Schmid & Casey (1986) (Fig. 7) and a typical olivine fabric from a deformed gabbro (Benn *et al.* 1988) (Fig. 8). The quartz *c*-axis fabric is

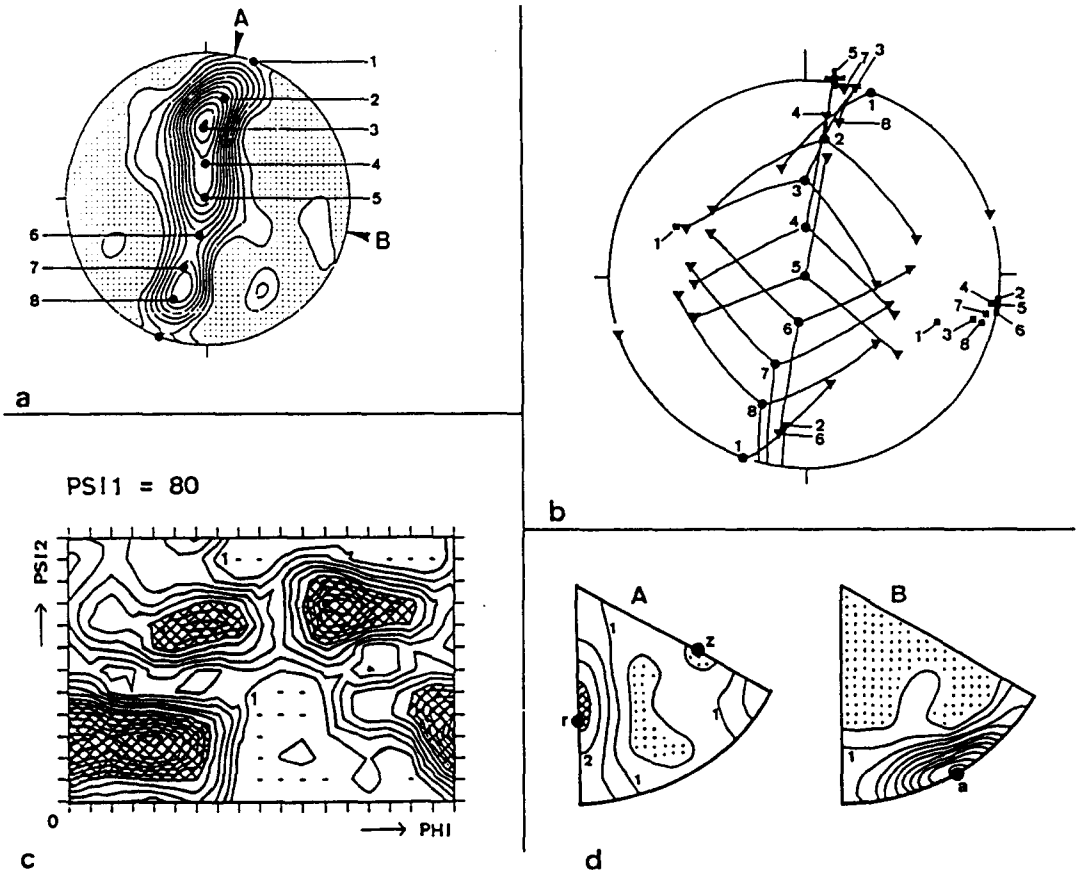

Fig. 7. A complete fabric analysis of quartz using the ODF technique from Schmid & Casey (1986). (a) Pole figure for the *c*-direction (contour interval 1.0) indicating and numbering the *c*-axis positions of crystal orientations chosen for the construction in (b). Specimen directions A (normal to the shear plane) and B (shearing direction) were used for the calculation of the inverse pole figures shown in (d). (b) Favoured crystal orientations for selected *c*-axis positions shown in (a). Dots = *c*-axis; triangles = poles to positive rhombs; squares = one of the three ⟨*a*⟩ directions; pole to the first-order prism of *c*-axis in position 5. (c) Section through the ODF at psi1 = 80°, corresponding to *c*-axis girdle marked by A in (a). (d) Inverse pole figures for the specimen directions A and B in (a). Note the strong concentrations of directions A near the negative rhomb (*r*) and directions B near the ⟨*a*⟩ axis.

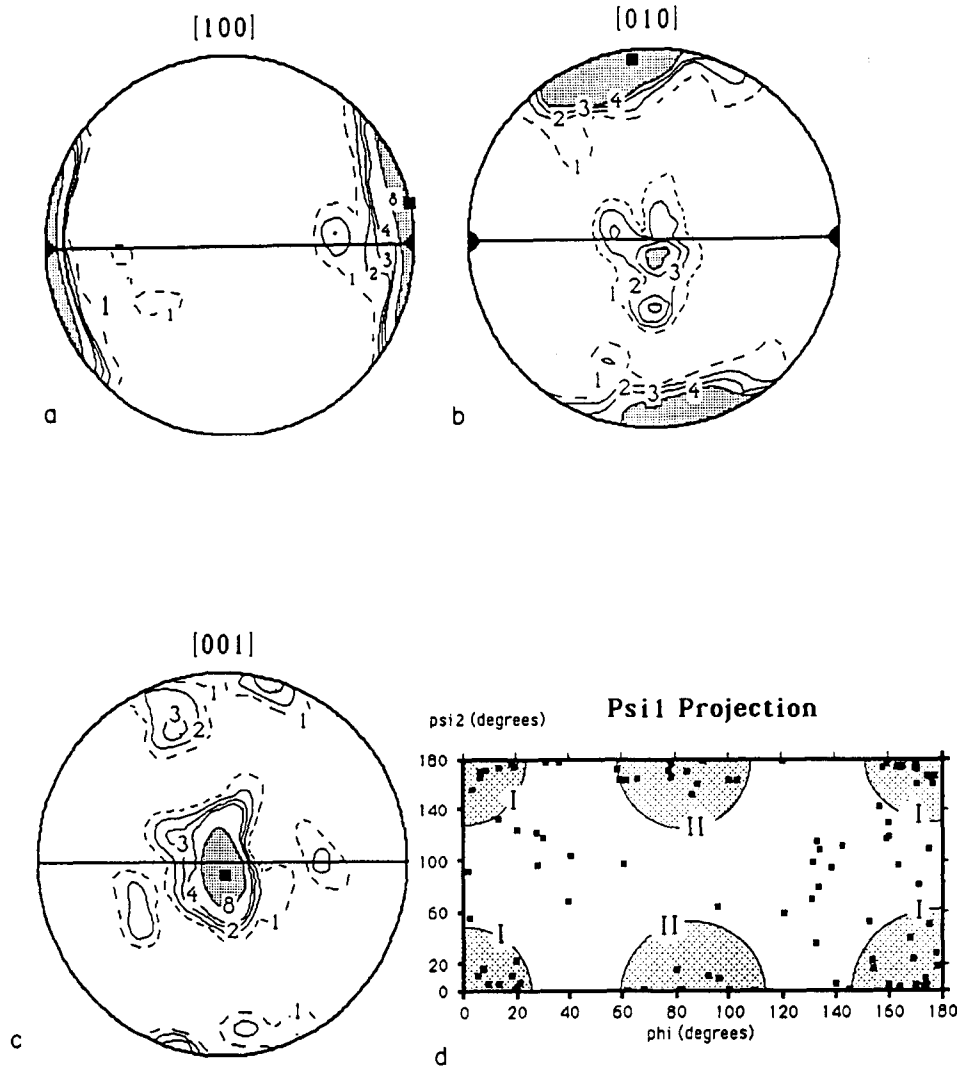

Fig. 8. Petrofabrics of olivine from a deformed dunite from the Wadi Fayd, Oman. (a)–(c) [100], [010] and [001] pole figures with the foliation (horizontal solid line) and lineation (black semi-circle) indicated. Contours in multiples of a uniform distribution, black square indicates maximum density. (d) ODF projection in the psi1 direction of individual crystal orientations (black squares). Note the two strong concentrations at (I) psi1 = 90°, phi = 0° (or 180°), psi2 = 0° (or 180°) and (II) psi1 = 90°, phi = 90°, psi2 = 90°.

recalculated from the ODF, itself derived from X-ray pole figures. The two maxima in the *c*-axis pole figure correspond to maxima in the ODF at (psi1 = 80°, phi = 40°, psi2 = 30°) and (psi1 = 80°, phi = 130°, psi2 = 90°) which means that *a*-axes are close to the lineation and the rhombohedral planes almost coincident with the pole to the foliation. Such an orientation is consistent with ⟨*a*⟩ (*r*) glide; such an interpretation is not intuitively obvious from the rhombohedral pole figures of this sample. In our second example (Fig. 8) (one of a few hundred olivine fabrics recorded in our institute over the last 20 years), the measurements were made with a universal stage. From the measurement of the optical indicatrix, the orientation of [100], [010] and [001] can be directly inferred, and hence the Bunge Euler angles can be calculated for each individual crystal. The [100] directions lie close to the lineation and the (001) planes almost coincident with the foliation (Fig. 8). In the ODF, concentrations occur at psi2 = 0°,180°,psi1 = 90° and phi = 0°,90°,180°, indicating [100] close to the lineation and [001] either normal to the foliation or in the foliation. Slip could be inferred to have occurred on [100] (001) or [100] (010) in individual grains. The microstructure of the individuals in these orientations can now be studied to investigate this possibility. The psi1 projection of this sample reveals many grains that are not in one of the two 'favoured' orientations.

LPO OF LOWER CRUST MINERALS

The principal minerals of granulite and amphibolite facies rocks exposed in lower crustal sections are plagioclase, pyroxene, amphibole, quartz and biotite, although where basic rocks are present olivine is locally important (e.g. the Alpine Ivrea zone, Fountain 1976) and occasionally carbonates in some sections. We will pay particular attention to the fabrics of plagioclase, pyroxene and amphibole, and briefly review quartz and olivine. Further information can be found in the literature about quartz (Schmid & Casey 1986), olivine (Nicolas & Poirier 1976, Mercier 1985) and carbonates (Wenk 1985, Wenk *et al.* 1987).

Plagioclase

Plagioclase is volumetrically the most important mineral in the crust, and the feldspar group as a whole constitutes over 51% of the crust (Ronov & Yowoshevsky 1969). Because of its triclinic symmetry, LPO studies of plagioclase have until recently been confined to reports of optical indicatrix fabrics (e.g. Shelley 1977, Jensen & Starkey 1985, Olsen & Kohlstedt 1985). The optical indicatrix does not coincide with simple crystallographic directions in triclinic minerals, hence our knowledge of the true LPO is extremely limited. Wenk *et al.* (1986) introduced a scheme to measure the complete preferred orientation of plagioclase from optical measurements on an orientation diagram constructed by Burri *et al.* (1967). This analysis requires the measurement of two planes (e.g. (010) and (001) cleavages), or albite and pericline twin planes (Ji & Mainprice 1988) and the optical indicatrix. The analysis allows the simultaneous determination of the crystallographic signs of the axes and the composition. The use of the two cleavages alone allows the construction of the crystallographic axes (e.g. Kruhl 1987). These workers show in particular that (010) is nearly always sub-parallel to the foliation with either [001] or [100] forming a maximum near the lineation. TEM work by Montardi & Mainprice (1987) and Ji & Mainprice (1988) has shown that [001] (010) slip with subsidiary [100] (010) is most important in these deformed specimens. Furthermore, Kruhl (1987) has reported a fabric with (001) sub-parallel to the foliation and [100] sub-parallel to the lineation, which he suggested may be due to [100] (001) slip in higher temperature conditions, a proposition which is consistent with experimental work on slip in potassium feldspars (Gandais & Williame 1984).

The overall view that (010) tends to be parallel to the foliation and either [100] or [001] sub-parallel to the lineation can also be inferred from earlier optical indicatrix fabrics (α [100], β (001), γ (010), for An_{20-30}) (e.g. Shelley 1977). A similar fabric also occurs in viscously deformed granites (An_{10}, Bouchez *et al.* 1981) and anorthosites (An_{75}, Munch 1988), hence great care must be used in assigning a mechanism of orientation to plagioclase rocks.

Pyroxene

A large number of pyroxene fabrics have been measured, exclusively by optical techniques (Mercier 1985). The majority of measurements have been made in mantle-derived rocks (peridotites, pyroxenites, eclogites) either tectonically or volcanically (xenoliths) emplaced in the continental crust. The fabrics found in nature can be conveniently classified into two groups by the crystallographic plane which is parallel to the foliation; group 1 has (100), and group 2 (010). The (100) fabric is commonly observed in orthopyroxenes from ophiolite complexes (e.g. Boudier 1978, Mercier 1985) with [001] parallel to the lineation and [010] in the foliation normal to the lineation (see Fig. 15 later). The (010) fabrics are particularly common in the clinopyroxene omphacite from eclogites where the (010) pole may form a girdle about the lineation (the 'L-type' of Helmstaedt *et al.* 1972). [001] is parallel to the lineation. The (010) pole may also form a girdle in the foliation ('S-type' of Helmstaedt *et al.* 1972). Typical examples of these fabrics can be seen in Van Roermund (1983). (010) fabrics in chrome diopside have also been reported by Boudier (1978) in deformed clinopyroxenite bands from the Alpine Lanzo massif.

Experimental studies have shown that glide on (100) [001] is the dominant high temperature (low stress) slip system in ortho- and clino-pyroxene (Avé Lallemant 1978, Ross & Nielsen 1978). The (100) [001] slip system is concordant with the observed (100) fabrics and microstructures. Detailed TEM studies of omphacite from deformed eclogites in specimens that have the (010) fabric (Van Roermund & Boland 1981, Van Roermund 1983) have shown extensive evidence for dominant {110} [001] slip with minor (100) [001] and {110} [110], but not (010) [001] as might have intuitively been expected. From a consideration of crystal chemistry, we expect a greater diversity in clinopyroxene slip systems compared to orthopyroxene (Doukhan *et al.* 1986); in particular, slip on (100) should play a less important role in clinopyroxene, as observed by Van Roermund (1983). However, we should note that in some naturally and experimentally deformed orthopyroxenes, Naze *et al.* (1987) have observed (010) [001]. Apart from these glide fabrics, a (010) fabric in orthopyroxene with [100] and [001] forming girdles in the foliation has been reported in Jackson's (1961) analyses of the Stillwater complex. In this case the bronzite grains of prismatic forms ($a:b:c = 0.67:0.39:1$) were orientated by a viscous flow mechanism. Benn & Allard (in press) have observed a similar fabric in clinopyroxene from a viscously deformed gabbro.

Amphibole fabrics

Relatively few fabrics have been reported. Most observations record a strong concentration of *c*-axes parallel to the lineation (e.g. Schwerdtner 1964, Gapais & Brun 1981, Rousell 1981). A preliminary X-ray fabric of two amphibolites by Kern & Fakhimi (1975) also revealed *c*-axes confined to the foliation plane with a concentration of (110) planes parallel to the foliation, and similar results were obtained by Gapais & Brun (1981). Our own observations (Fig. 16, later) show a fabric with (100) parallel to the foliation and [001] parallel to the lineation.

Schwerdtner (1964) suggested that amphibole fabrics developed under non-hydrostatic stress in the manner proposed by Kamb's (1959) thermodynamic theory. However, this has been criticized by Helmstaedt *et al.* (1972), as similar fabrics occur in minerals with differing elastic properties, contrary to the predictions of Kamb's theory. From an inspection of the amphibole structure one would predict that easy glide occurs on the (100) [001] system as this does not break any strong Si–O

bonds. Such slip has been experimentally observed by Rooney & Riecker (1969, 1973) and inferred from optical measurements by Dollinger & Blacic (1975). More recently Biermann & Van Roermund (1983) studied naturally deformed clino-amphiboles by TEM and observed evidence for (hk0) [001] slip. However evidence for plasticity is often lacking in amphibole crystals from deformed metamorphic rocks (Rooney *et al.* 1975) and they may often act as rigid inclusions in a more ductile matrix (see data of Rousell 1981).

Quartz

In this section we will not review all aspects of quartz LPO, but rather concentrate on the fabric transitions in shear deformation and the possible physical reasons for these transitions. Like calcite (see Wenk *et al.* 1987), quartz often deforms by slip on several slip planes. The variation of the critical resolved shear stress as a function of temperature can be deduced from the experimental work on single crystals of Hobbs *et al.* (1972), Blacic (1975) and Linker & Kirby (1981) (see Fig. 9—based on the compilation of Hobbs 1985). In an intuitive manner, one can predict that various fabric regimes will occur on a constant strain-rate contour (dashed line in Fig. 9) in the stress–temperature space. A more mathematical approach can be used to model such fabric transitions using the Taylor theory (e.g. Lister & Paterson 1979) within the limitations of that model (see above). In our schematic Fig. 9, the glide at low temperature is on the basal plane in ⟨*a*⟩ direction; with increasing temperature, the dominant glide activity moves to prismatic planes and eventually to the [*c*] direction. Why does this transition occur? The answer comes essentially from the experimental work of Blacic (1975) and Linker & Kirby (1981) who noted that in synthetic quartz glide was particularly easy in the [*c*] direction. Linker & Kirby (1981) proposed that the different glide rates in the ⟨*a*⟩ and [*c*] directions were related to an anisotropy of diffusion along these directions. Subsequent work of

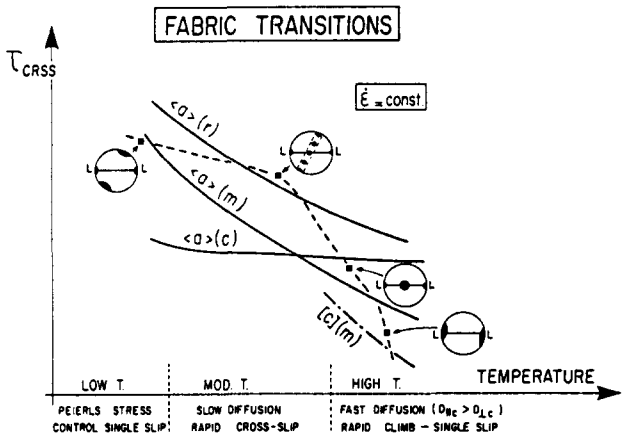

Fig. 9. Fabric transitions in quartz after Hobbs (1985). A schematic transition diagram showing the variation of the critical stress to activate ⟨*a*⟩ (*r*) ⟨*a*⟩ (*c*) and [*c*] (*m*) glide in quartz for a constant strain rate as a function of temperature. The dashed line represents the strength and fabric transitions of a hypothetical polycrystal.

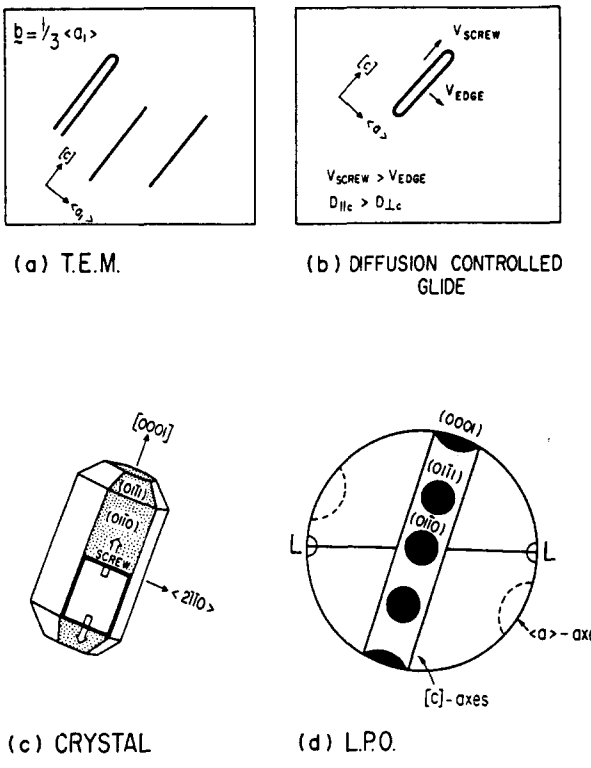

Fig. 10. Schematic relationship between dislocation microstructure and LPO in quartz. (a) TEM microstructure; (b) interpretation in terms of anisotropic diffusion-controlled glide; (c) crystal with cross-slipping screw dislocation; (d) simplified LPO of quartz.

Dennis (1984) and Giletti & Yund (1984) confirmed that oxygen diffusion was much faster in the [*c*] direction than the ⟨*a*⟩ direction. Linker *et al.* (1984) showed by TEM that dislocations in samples deformed in orientations for ⟨*a*⟩ and [*c*] slip had their line directions predominantly parallel to [*c*]. In our Fig. 10(a), we schematically illustrate this microstructure and its interpretation in terms of diffusion-controlled glide Fig. 10(b). Once it has been shown that screw dislocations with 1/3 [*a*] Burgers vectors can glide more rapidly than edge orientations, it is straightforward to make a correlation between the *c*-axis girdle fabric (Fig. 10d) and a crystal deforming by a rapid cross-slip mechanism (Fig. 10c). Increasing the temperature will increase the importance of diffusion in the [*c*] direction and hence the velocity of dislocation glide in that direction and on planes containing it. Hence the prism slip plane and [*c*] slip direction become more active with increasing temperature. For example, quartz *c*-axis fabrics from a gneiss series deformed at high temperature on the Red Sea Zabargad Island (Ji *et al.* 1988) show considerable topological variations consistent with ⟨*a*⟩ (*r*) and [*c*] (*m*) slip, whereas the plagioclase (010) pole figures did not vary. The temperature sensitivity of glide in quartz probably reflects to a large extent the importance of diffusion (lattice and pipe) in the hydrolytic or water weakening process so intimately associated with the plasticity of quartz. The anisotropy of the glide process has not yet been fully taken into account in fabric modelling.

T domains	dominant slip systems	Fabrics strength, type	Relation with flow plane (horizontal) and flow line (arrow)
⩾1250°C (hypersolidus)	(010) [100] (001) [100]	- extreme - point maxima partial girdles	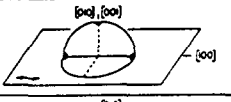
>1100°C (high-T)	(010) [100]	- strong - point maxima	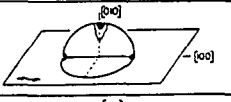
~1000°C (medium-T)	(0kl) [100]	- distinct - point maximum and girdle	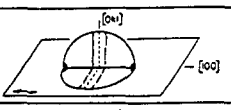
700-1000°C (low-T)	(0kl) [100] (010) [001]	- absent or weak - double diffuse girdle	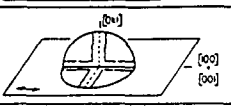

Fig. 11. Fabric variation in olivine as a function of temperature.

Olivine

At lower crust temperatures (600–800°C) olivine is at the lower temperature limit of plasticity. However as segments of mantle rocks are often tectonically included, as peridotite massifs, in lower crustal sections, we have included here a brief review of the typical LPO patterns. The experimental work of Carter & Avé Lallemant (1970) has shown that different slip systems are activated in olivine as a function of temperature. Studies on naturally deformed peridotites conducted by Nicolas and co-workers (e.g. Nicolas *et al.* 1973) confirm this and make it possible to estimate the temperature domains using petrological geothermometers and partial melting evidence; the results are presented in Fig. 11. At very high temperatures, fabrics can be extremely strong due to enhanced diffusion and grain-boundary mobility selecting the favourably oriented grains.

RELATIONSHIP BETWEEN LPO AND SEISMIC ANISOTROPY

In many seismic sections of the continental crust, the upper crust and mantle are transparent whereas the lower crust is strongly reflective (Fig. 1) (see Moody & Brocher 1987 for review). The reflective lower crust is seismically laminated and the origin of these laminations is one of the most important questions posed by the deep crustal seismic programs (COCORP, ECORS, BIRPS, etc.). The laminated sections are continuous over tens of kilometers and 5 km or more thick. It is clear that they represent a major zone of anisotropy. From the evidence of vertical to wide-angle reflections (Fuchs *et al.* 1987) and synthetic seismograms (Sandmeier & Wenzel 1986, Hurich & Smithson 1987), the laminations have been ascribed a thickness of 35–150 m with alternating high velocity (7.2 km s^{-1}) and low velocity (6.2 km s^{-1}) layers of a solid-state nature. Various interpretations have been proposed to explain this lamination: intrusion of mafic igneous sills (e.g. Finlayson *et al.* 1984); ductile shear flow (e.g. Klemperer 1987); high pore fluid pressures close to faults, reducing the V_p values (Jones & Nur 1984). We wish to investigate the influence of fabrics on this laminar character of the lower crust.

In order to calculate the seismic anisotropy of deformed rock, we need to study samples within their tectonic framework (lineation–foliation). In most of the laboratory measurements, attention has been paid to the foliation and two orthogonal directions in the foliation. However to allow a full exploitation of the data in a more general geodynamic context, care must be taken to relate properties to both foliation and lineation (e.g. Peselnick *et al.* 1974). To calculate the seismic properties of an aggregate, we must know the LPO, density, single crystal elastic stiffness coefficients and volume fraction of each mineral. The calculated seismic properties may be extrapolated to any temperature or pressure of interest if the appropriate temperature and pressure derivatives are available. Details of the calculation procedure can be found in Peselnick *et al.* (1974). The calculation yields a complete projection for any of the seismic velocities V_p, V_s, V_{ss} as well as the difference in shear wave velocity or 'shear wave splitting' $\Delta V_s = | V_s - V_{ss} |$, which can be used as a seismic diagnostic of anisotropy (Crampin 1984). The major advantages of this approach are:

(a) a clear relation is established between LPO and seismic anisotropy;

(b) the contribution of each mineral to the anisotropy can be directly assessed; and

(c) the velocity values are calculated over a complete hemisphere projection, not just in three orthogonal directions.

The major disadvantages of this technique are that:

(a) it requires volumetric sampling of LPO, a condition more rigourously fulfilled by X-ray or neutron texture goniometry, and

(b) it relies on the quality of the available elastic constants and their derivatives.

Fabrics, seismic anisotropy and the lamination of the lower crust

In this section we will illustrate the role of mineralogy and LPO on the seismic anisotropy of two typical lower-

crustal rock compositions. We have chosen quartz, plagioclase diopside and hornblende as the volumetrically important minerals, but we have not considered garnet as it is elastically isotropic and hence does not contribute to the seismic anisotropy. Adding garnet to our hypothetical rocks would increase the seismic velocities as garnet is an extremely dense mineral and would dilute the anisotropy. We have also not considered biotite which is very anisotropic because it is volumetrically much less important in the deep crust; in more shallow crustal rocks it is known to be an important contributor to rock anisotropy (Jones & Nur 1984).

Anisotropy of single crystals

Before considering the anisotropy derived from polycrystals it is important to have in mind the properties of the single crystal. The P-wave velocity projections for quartz, plagioclase (An_{53}), diopside and hornblende are shown in Fig. 12, calculated from the elastic constants given by Aleksandrov *et al.* (1974) for plagioclase, diopside and hornblende, and McSkimin *et al.* (1965) for quartz. The symmetry of the P-wave contours faithfully reflects the crystal symmetry of each mineral, except for plagioclase where the original elastic data have been reduced in a monoclinic reference frame (see Aleksandrov *et al.* 1974 for discussion). Diopside and hornblende have similar anisotropies with a maximum V_p near the *c*-axis. Plagioclase has a maximum V_p parallel to the *b*-axis with a minimum near the *a*-axis. Finally quartz has a maximum near the pole to the rhombohedral plane. The seismic anisotropies (A) (where $A = (V_{max} - V_{min}) / V_{max}$) of these minerals are: quartz, A=24.4%; plagioclase, A=27.4%; diopside, A=23.1%; hornblende, A=23.9%. These values can be compared with A=21.8% for olivine and A=11.3% for enstatite, the two minerals that give rise to the seismic anisotropy of the upper mantle (Nicolas & Christensen 1987). The minerals of the lower crust must be regarded as extremely anisotropic.

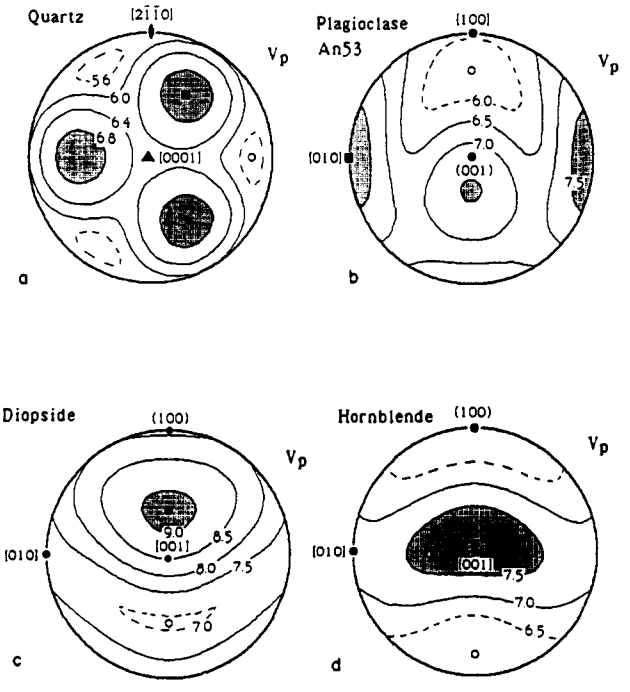

Fig. 12. Upper-hemisphere stereograms of P-wave velocities for single crystals of quartz, plagioclase, diopside and hornblende, with the elastic X_1 axis = north, X_2 = east and X_3 vertical (origin). Contours in km s^{-1}.

Quartz

The complete orientation of quartz cannot be measured by optical means, except where second-order prism sub-boundaries are present (Bouchez 1977) and even this has to be verified by diffraction methods. To calculate the seismic anisotropy we need the ODF which can be derived from X-ray or neutron texture goniometry. We illustrate seismic P-wave anisotropy of typical quartz fabric which has been calculated from ODF of Dervin & Bouchez (unpublished data 1979) (Fig. 13) derived from neutron diffraction, which has the distinct advantage over X-rays of sampling a large volume (1 cm^3). The V_p distribution reflects concentration of *a*-axes (low velocity directions) near the lineation. A broad band of high V_p (6.2 km s^{-1}) occurs in the central region. The V_p anisotropy of the polycrystal is 6%, much lower than the single-crystal value. LPOs with single *c*-axes maxima either parallel to the lineation (X) or normal to the lineation in the foliation plane (Z) are likely to produce higher anisotropies.

Plagioclase

Our plagioclase example (Fig. 14) is taken from the work of Ji & Mainprice (1988). The fabric shows typical pattern dominated by the *a*-axes normal to the lineation in the foliation (Y) and *b*-axes parallel to the pole to the foliation (Z). The V_p distribution faithfully reflects the LPO, in particular the minimum velocity at Y and a maximum near Z. The anisotropy coefficient is 13%, a high value essentially being produced by the strong maximum of *a*-axes (8.3 multiples of a uniform distribution).

Diopside

Our diopside example (Fig. 15), whose associated plagioclase fabric was studied in Ji & Mainprice (1988) has a typical pyroxene fabric with (100) parallel to the foliation (Z) and [001] to the lineation (X). The V_p distribution shows a maximum parallel to the lineation and a minimum near Z. The anisotropy coefficient is only 5%, principally due to the relatively diffusive fabric of the a^* and *c* axes (6 times uniform).

Hornblende

The hornblende example (Fig. 16) comes from a rock with an identical feldspar fabric to Fig. 14. The fabric is very similar to that of diopside, but the maxima of a^* and *c* are much more pronounced (9 and 10 times uniform). The V_p distribution is similar to diopside except the

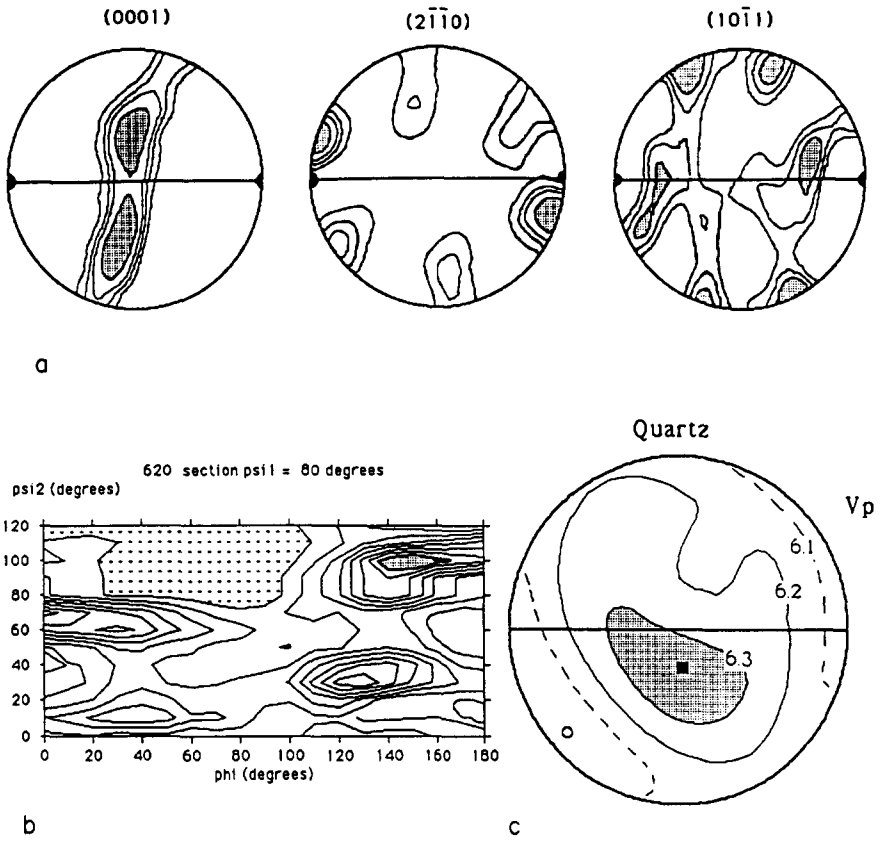

Fig. 13. LPO of a quartzite (Dervin & Bouchez 1979 unpublished data) and the corresponding P-wave variation. (a) (0001), (2$\bar{1}\bar{1}$0) and (10$\bar{1}$1) pole figures generated from the ODF. Contours in times uniform. (b) Contoured ODF section at psi1=80°. Contours in times uniform at intervals of 2, with the region above 16 shaded. (c) P-wave lower-hemisphere stereogram contoured in km s^{-1}.

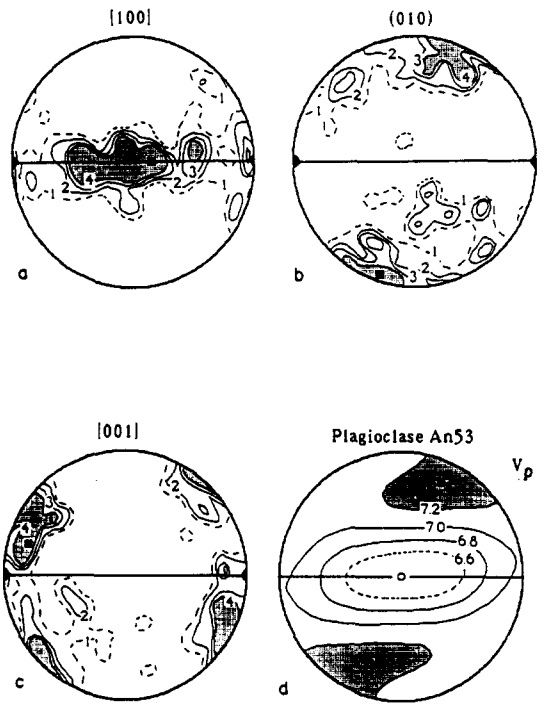

Fig. 14. Plagioclase LPO and P-wave variation: (a) [100] pole figure, contours in times uniform; (b) (010) pole figure, contours in times uniform; (c) [001] pole figure, contours in times uniform; (d) P-wave stereogram, contours in km s^{-1}.

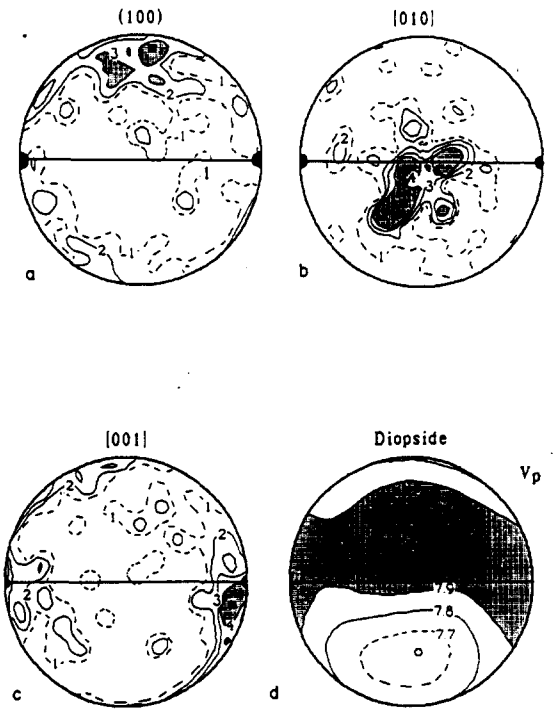

Fig. 15. Diopside LPO and P-wave variation: (a) (100) pole figure, contours in times uniform; (b) [010] pole figure, contours in times uniform; (c) [001] pole figure, contours in times uniform; (d) P-wave stereogram, contours in km s^{-1}.

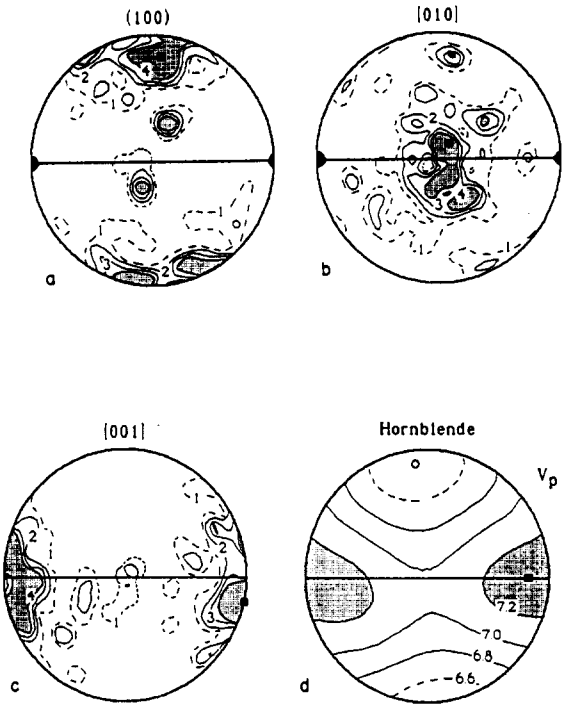

Fig. 16. Hornblende LPO and P-wave variation: (a) (100) pole figure, contours in times uniform; (b) [010] pole figure, contours in times uniform; (c) [001] pole figure, contours in times uniform; (d) P-wave stereogram, contours in km s^{-1}.

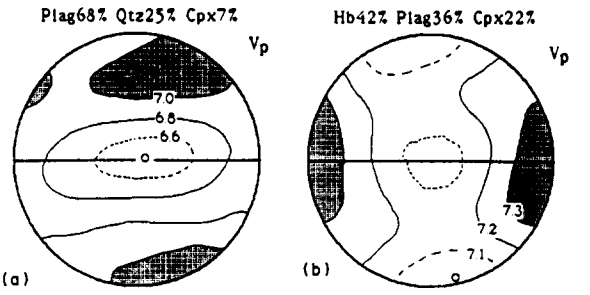

Fig. 17. P-wave variation in two hypothetical rocks, contours in km s^{-1}. (a) Rock composition of specimen 1 of Christensen & Fountain (1975) rounded to 100% (quartz 25%, plagioclase 68%, diopside 7%). They recorded velocities in three orthogonal directions at 600 MPa confining pressure of 6.48, 6.64 and 6.59 km s^{-1}. (b) Rock composition of specimen 9 of Christensen & Fountain (1975) rounded to 100% (plagioclase 36%, hornblende 42%, diopside 7%). They recorded velocities in three orthogonal directions at 600 MPa confining pressure of 7.31, 7.61 and 7.17 km s^{-1}.

anisotropy coefficient of 12% is less than plagioclase but significantly greater than our pyroxene example.

Anisotropy of rock

Once we have LPO data for each mineral we can combine them together with the elastic constants to produce the seismic velocity data for any composition. Here we will limit ourselves to two rock compositions reported by Christensen & Fountain (1975) for granulites (their samples 1 and 9). In the first example (Fig. 17a) with 25% quartz, 68% plagioclase and 7% diopside, the V_p anisotropy coefficient is 9% with high velocities near X and Z and a low velocity at Y. The mean V_p velocity is 6.8 km s^{-1}, similar to that found in the lower velocity layer in the seismically laminated lower crust. In our second example (Fig. 17b) with 36% plagioclase, 42% hornblende and 22% diopside, a very different velocity distribution is produced and the anisotropy coefficient is only 5%. A high V_p value still occurs at X and a low V_p value at Y but now the lowest V_p value occurs at Z. The mean V_p for this composition is 7.2 km s^{-1}, similar to higher velocity layer in the laminated lower crust. These examples illustrate the relatively complex interaction between the anisotropies of the various minerals. The V_p anisotropy of each of the minerals is between 23 and 28%, hence the bulk anisotropy of a rock will simply reflect the relative volume and orientation of each mineral.

Plagioclase, diopside and hornblende have simple V_p distributions. However as the [100] of plagioclase (low velocity) and [010] of pyroxenes and amphiboles (moderate velocity) are commonly in the foliation and normal to the lineation in typical fabric diagrams, their summed contribution tends to reduce the seismic anisotropy. Some highly deformed lower crustal rocks have random fabrics due to superplastic deformation (Boullier & Gueguen 1975, Jensen & Starkey 1985, Behrmann & Mainprice 1987), so these zones are expected to have no seismic anisotropy and a seismic velocity which is uniquely determined by the composition. In the case of a monomineralic plagioclase rock (Fig. 14), our most anisotropic example, the P-wave velocity varies between 6.4 and 7.2 km s^{-1}, whereas a calculated random fabric gives 6.8 km s^{-1}. Hence, assuming a horizontal layering of plagioclase rocks with alternating strong fabrics (plastic deformation) and random fabrics (superplastic deformation), the maximum difference in seismic velocity between the layers would be 0.4 km s^{-1} or an anisotropy of 6%. Seismic modelling suggests that the velocity difference between the observed seismic laminations is 1.0 km s^{-1} or an anisotropy of 14%, so if the modelling is correct some compositional variations or other factors must intervene to increase the anisotropy.

CONCLUSIONS

We have reviewed the origin of LPO by plastic and viscous flow, applied it to lower-crustal minerals and examined its potential application to the seismic anisotropy of the continental lower crust. The lower crust is often seismically reflective with a laminated structure. In extensional regions, it is certain that this crust has been actively deformed by plastic and viscous deformation (Fig. 1) and hence it is reasonable to ask if the seismic lamination can be explained by the action of deformation recorded by the fabrics (LPOs). We have shown that strong LPOs exist in the main rock-forming minerals of the lower crust and that these minerals are extremely seismically anisotropic. Synthetic V_p diagrams of various compositions illustrate the interaction between the LPO of each mineral and their contribution to the total rock anisotropy. The addition of several minerals reduces the

anisotropy, the highest values being formed in monomineralic aggregates of plagioclase. The presence or absence of LPO alone, for example in adjacent layers deforming of highly anisotropic plagioclase by the plastic and superplastic modes, can only produce an anisotropy of 6%, whereas modelling of the laminations represents an anisotropy of 14%. Layers of alternating plagioclase fabric result in normal incidence P-wave reflection coefficients of 0.03–0.05, very similar to values estimated for compositional layering (Hurich & Smithson 1987). We suggest that a combination of other factors, such as composition, the effect of anisotropy on reflection coefficients (Daley & Hron 1979) or constructive interference effects (Blundell & Raynaud 1986, Hurich & Smithson 1987) could be responsible for increasing the anisotropy to the observed value. Such effects are complex and require detailed modelling with synthetic seismograms to distinguish between the geometrical effects and those due to variations in physical properties. That deformation fabrics alone cannot be responsible for the laminations seems to be confirmed by the absence of laminations in upper mantle which has a strong seismic anisotropy due to deformation-induced fabrics.

The application of our knowledge of seismic anisotropy resulting from LPOs to the kinematics of the lower crust awaits regional seismic studies of anisotropy currently being undertaken in many parts of the world. Studies by structural geologists of exposed sections of the lower crust, combined with physical measurements (e.g. Fountain 1976, Kern & Schenk 1988), calculations of seismic properties from LPOs (e.g. Ji & Mainprice 1988) and calculation of seismic profiles using synthetic seismograms (e.g. Hurich & Smithson 1987), should reveal valuable information on the still mysterious laminated lower crust.

Acknowledgements—We thank P. Dervin and J.-L. Bouchez for access to their unpublished quartz diffraction data, and K. Benn and S. Ji for U-stage data. Reviews by M. Casey, J. Hall, N. Kusznir and S. Treagus helped improve the presentation. Special thanks to S. Treagus for her editorial patience. The financial support of the 'ATP-Accompagnement ECORS 87' for the velocity and ODF calculations is duly acknowledged.

REFERENCES

Aleksandrov, K. S., Alchikov, U. V., Belikov, B. P., Zaslavskii, B. I. & Krupnyi, A. I. 1974. Velocities of elastic waves in minerals at atmospheric pressure and increasing precision of elastic constants by means of EVM (in Russian). *Izv. Acad. Sci. URSS, Geol. Ser.* No.10, 15–24.

Arzi, A. A. 1978. Critical phenomena in the rheology of partially melted rocks. *Tectonophysics* **44**, 173–184.

Avé Lallemant, H. G. 1978. Experimental deformation of diopside and websterite. *Tectonophysics* **48**, 1–27.

Behrmann, J. H. & Mainprice, D. 1987. Deformation mechanisms in a high temperature quartz-feldspar mylonite; evidence for superplastic flow in the lower continental crust. *Tectonophysics* **140**, 297–305.

Benn, K. & Allard, B. In press. Preferred mineral orientations related to magnetic flow in ophiolite layered gabbros. *J. Petrol.*

Benn, K., Nicolas A. & Reuber I. 1988. Mantle–crust transition zone and origin of wehrlitic magmas: evidence from the Oman ophiolite. *Tectonophysics* **151**, 75–85.

Biermann, C. & Van Roermund, H. L. M. 1983. Defect structures in naturally deformed clinoamphibole. A TEM study. *Tectonophysics* **95**, 267–278.

Blacic, J. D. 1975. Plastic deformation mechanisms in quartz: the effect of water. *Tectonophysics* **27**, 271–294.

Blumenfeld, P. 1983. Le "tuilage des mégacristaux", un critère d'écoulement rotationnel pour les fluidalités des roches magmatiques: application au granite de Barbey-Séroux (Vosges, France). *Bull. Soc. géol. Fr.* **25**, 309–318.

Blumenfeld, P. & Bouchez, J. -L. 1988. Shear criteria in granite and migmatite deformed in the magmatic and solid states. *J. Struct. Geol.* **10**, 361–372.

Blundell, D. J. & Raynaud, B. 1986. Modeling lower crust reflections observed on BIRPS profiles. In: *Reflecting Seisimology, A Global Perspective* (edited by Barazangi, M. & Brown, L.). *Am. Geophys. Un. Geodyn. Ser.* **13**, 287–295.

Bouchez, J. -L. 1977. Plastic deformation of quartzites at low temperature in an area of natural strain gradient. *Tectonophysics* **39**, 25–50.

Bouchez, J.-L. & Duval, P. 1982. The fabric of polycrystalline ice deformed in simple shear-experiments in torsion, natural deformation and geometrical interpretation. *Textures Microstruct.* **5**, 171–190.

Bouchez, J.-L., Guillet, P. & Chevalier, F. 1981. Structures d'écoulement liées à la mise en place du granite de Guérande (Loire-Atlantique, France). *Bull. Soc. géol. Fr.* **23**, 387–399.

Bouchez, J.-L., Lister, G. S. & Nicolas, A. 1983. Fabric asymmetry and shear sense in movement zones. *Geol. Rdsch.* **72**, 401–419.

Boudier, F. 1978. La massif Iherzolitique de Lanzo (Alpes Piemontaises) etude structurale et petrologique. Unpublished these d'Etat, Université de Nantes.

Boullier, A. M. & Gueguen, Y. 1975. Sp-mylonites: origin of some mylonites by superplastic flow. *Contr. Miner. Petrol.* **502**, 93–104.

Bunge, H. J. 1982. *Texture Analysis in Materials Science.* Butterworths, London.

Burri, C., Parker, R. L. & Wenk, E. 1967. *Die Optische Orientieryng der Plagiokase.* Birkhaüsse, Basel.

Carter, N & Avé Lallemant, H. G. 1970. High temperature flow of dunite and peridotite. *Bull. geol. Soc. Am.* **81**, 2181–2202.

Christensen, N. I. & Fountain, D. M., 1975. Constitution of the lower crust based on experimental studies of seismic velocities in granulite. *Bull. geol. Soc. Am.* **86**, 227–236.

Crampin, S. 1984. An introduction to wave propagation in anisotropic media. *Geophys. J. R. astr. Soc.* **76**, 17–28.

Daley, P. F. & Hron, F. 1979. Reflection and transmission coefficients for seismic waves in ellipsoidally anisotropic media. *Geophysics* **44**, 27–38.

Dennis, P. F. 1984. Oxgen self-diffusion in quartz under hydrothermal conditions. *J. geophys. Res.* **89**, 4047–4057.

Den Tex, E. 1969. Origin of ultramatic rocks, their tectonic setting and history. *Tectonophysics* **7**, 457–488.

Dollinger, G. & Blacic, J. D. 1975. Deformation mechanisms in experimentally and naturally deformed amphiboles. *Earth. Planet. Sci. Lett.* **26**, 409–416.

Doukhan, J.-C., Doukhan, N., Naze, L. & Van Duysen, J.-C. 1986. Défauts de réseau et plasticité cristalline dans les pyroxénes: une revue. *Bull. Minéral.* **109**, 377–394.

Duffield, W. A. 1968. The petrology and structure of the El Pinal tonalite, Baja California, Mexico. *Bull. geol. Soc. Am.* **79**, 1351–1374.

Etchecopar, A & Vasseur, G. 1987. A 3-D kinematic model of fabric development in polycrystalline aggregates: comparisons with experimental and natural examples, *J. Struct. Geol.* **9**, 705–717.

Fernandez, A., Feybese, J. L. & Mezure, J. F. 1983. Theoretical and experimental study of fabrics developed by different shaped markers in two-dimensional simple shear. *Bull. Soc. géol. Fr.* **25**, 319–326.

Finlayson, D. M., Collins, C. D. N. & Lock, J. 1984. P-wave velocity features of the lithosphere under the Eromanga Basin, Eastern Australia including a prominent mid-crustal (Conrad?) discontinuity. *Tectonophysics* **101**, 267–291.

Fountain, D. M. 1976. The Ivrea-Verbano and Strona-Ceneri zones, northern Italy: a cross-section of the continental crust — new evidence from seismic velocities of rock samples. *Tectonophysics* **33**, 145–165.

Fuchs, K., Bonjer, K. P., Gajewski, D., Lueschen, E., Prodehl, C., Sandmeier, K. J., Wenzel, F. & Wilhelm, H. 1987. Crustal evolution of the Rhinegraben area. I. Exploring the lower crust in the Rhinegraben rift by unified geophysical experiments. In: *Sedimentary Basins within the Dead Sea and Other Rift Zones* (edited by Ben-Avraham, Z.). *Tectonophysics* **141**, 261–275.

Gandais, M. & Willaime, C. 1984. Mechanical properties of feldspars. In: *Feldspars and Feldspathoids* (edited by Brown, W. L.), NATO ASI Ser., C-137. Reidel, Dordrecht, 207–246.

Gapais, D. & Brun, J. P. 1981. A comparison of mineral grain fabrics and finite strain in amphibolites from eastern Finland. *Can. J. Earth Sci.* **18**, 995–1003.

Giletti, B. J. & Yund, R. A. 1984. Oxygen diffusion in quartz. *J. geophys. Res.* **89**, 4039–4046.

Helmstaedt, H., Anderson, O. L. & Gavasci, A. T. 1972. Petrofabric studies of eclogite, spinel-websterite, and spinel-lherzolite xenoliths from kimberlite-bearing breccia pipes in south eastern Utah and Northeastern Arizona. *J.* geophys. Res. **77**, 4350–4365.

Hobbs, B. E. 1985. The geological significance of microfabric. In: *Preferred Orientation in Deformed Metals and Rocks* (edited by Wenk, H.-R.). Academic Press, Orlando.

Hobbs, B. E., McLaren, A. C. & Paterson, M. S. 1972. Plasticity of single crystals of synthetic quartz. In: *Flow and Fracture of Rocks* (edited by Heard, H. C., Borg, I. Y., Carter, N. I. & Raleigh, C. B.). *Am. Geophys. Un. Geophys. Monogr.* **16**, 29–53.

Hurich, C. A. & Smithson, S. B. 1987. Compositional variation and the origin of deep crustal reflections. *Earth Planet. Sci. Lett.* **85**, 416–426.

Jackson, E. D. 1961. Primary textures and mineral associations in the ultramafic zone of the Stillwater complex Montana. *Prof. Pap. U.S. geol. Surv.* **358**.

Jackson, E. D., Green, H. W. & Moores, E. M. 1975. The Vourinos ophiolite Greece: cycle units of lineated cumulates overlying harzburgite tectonite. *Bull. geol. Soc. Am.* **86**, 390–398.

Jeffrey, J. B. 1922. The motion of ellipsoidal particles immersed in a viscous fluid. *Proc. R. Soc. Lond.* **A102**, 161–179.

Jensen, L. N. & Starkey, J. 1985. Plagioclase microfabrics in a ductile shear zone from the Jotun Nappe, Norway. *J. Struct. Geol.* 7, 527–539.

Jessell, M. W. 1988. Simulation of fabric development in recrystallization aggregates — I. Description of the model. *J. Struct. Geol.* **10**, 771–778.

Ji, S. & Mainprice, D. 1988. Natural deformation fabrics of plagioclase: implications for slip systems and seismic anisotropy. *Tectonophysics* **147**, 145–163.

Ji, S., Mainprice, D. & Boudier, F. 1988. Sense of shear in high temperature movement zones from the fabric asymmetry of plagioclase feldspar. *J. Struct. Geol.* **10**, 73–81.

Jones, T. D. & Nur, A. 1984. The nature of seismic reflections from deep crustal shear zones. *J. geophys. Res.* **89**, 3153–3171.

Kamb, W. B. 1959. Theory of preferred orientation developed by crystallization under stress. *J. Geol.* **67**, 153–170.

Kern, H. & Fakhimi, M. 1975. Effect of fabric anisotropy on compressional wave propagation in various metamorphic rocks for the range 20–700°C at 2 kbars. *Tectonophysics* **28**, 227–244.

Kern, H. & Schenk, V. 1988. A model of velocity structure beneath Calabria, Southern Italy, based on Laboratory data. *Earth Planet. Sci. Lett.* **87**, 325–337.

Kirby, S. H. 1985. Rock mechanics observations pertinent to the rheology of the continental lithosphere and the localization of strain along shear zones. *Tectonophysics* **119**, 1–27.

Klemperer, S. L., 1987. Reflectivity of the crystalline crust: hypotheses and tests. *Geophys. J. R. astr. Soc.* **89**, 217–222.

Kruhl, J. H. 1987. Preferred orientations of plagioclase from amphibolite and greenschist facies rocks near the Insubric Line (Western Alps). *Tectonophysics* **135**, 233–242.

Law, R. D. 1987. Heterogeneous deformation and quartz crystallographic fabric transitions: natural examples from the Moine Thrust zone at the Stack of Glencoul, northern Assynt. *J. Struct. Geol.* **9**, 819–833.

Linker, M. F. & Kirby, S. H. 1981. Anisotropy in the rheology of hydrolytically weakened synthetic quartz crystals. In: *Mechanical Behavior of Crustal Rocks* (edited by Carter, R. L., Logan, J. M. & Stearns, D. W.). Am. Geophys. Un. Washington, D.C.

Linker, M. F., Kirby, S. H., Ord, A. & Christie, J. M. 1984. Effects of compression direction on the plasticity and rheology of hydrolytically weakened synthetic quartz at atmospheric pressure. *J. geophys. Res.* **89**, 4241–4255.

Lister, G. S. & Paterson, M. S. 1979. The simulation of fabric development during plastic deformation and its application to quartzite: fabric transitions. *J. Struct. Geol.* **1**, 99–115.

Lister, G. S., Paterson, M. S. & Hobbs, B. E. 1978. The simulation of fabric development in plastic deformation and its application to quartzite: the model. *Tectonophysics* **45**, 107–158.

McSkimin, H. J., Anreatch, P., Jr. & Thurston, R. N. 1965. Elastic moduli of quartz versus hydrostatic pressure at 25° and −195.8°C. *J. appl. Phys.* **36**, 1624–1632.

March, A. 1932. Mathematische Theorie der Regelung nach der Korngestalt bei affiner Deformation. *Z. Kristallogr.* **81**, 285–297.

Means, W. D. & Paterson, M. S. 1966. Experiments on preferred orientation of platey minerals. *Contr. Miner. Petrol.* **13**, 108–133.

Mercier, J. C. 1985. Olivine and pyroxenes. In: *Preferred Orientation in Deformed Metals and Rocks* (edited by Wenk, H.-R.). Academic Press, Orlando.

Montardi, Y. & Mainprice, D. 1987. A TEM study of the natural plastic deformation of calcic plagioclase (An 68–70). *Bull. Minéral.* **110**, 1–14.

Moody, W. D. & Brocher, T. M. 1987. Coincident seismic reflection/refraction studies of the continental lithosphere: a global review. *Rev. Geophys.* **25**, 723–742.

Munch, P. 1988. Etude de la deformation naturelle et experimentale de plagioclases. Unpublished DEA rapport, U.S.T.L., Montpellier.

Naze, L., Doukhan, N., Doukhan, J. C. & Latrons K. 1987. A TEM study of lattice defects in naturally and experimentally deformed orthopyroxenes. *Bull. Minéral.* **110**, 497–512.

Nicolas, A., 1987. *Principles of Rock Deformation.* Reidel, Dordrecht.

Nicolas, A., Bouchez, J.-L. & Boudier, F. 1972. Interprétations cinématiques des déformations plastiques dans le massif de lherzolite de Lanzo (Alpes Piémontaises), comparaison avec d'autres massifs. *Tectonophysics* **14**, 143–171.

Nicolas, A. & Christensen, N. I. 1987. Formation of anisotropy in upper mantle peridotites — a review. *Rev. Geophys.* **25**, 111–123.

Nicolas, A., Boudier, F. & Boullier, A. M. 1973. Mechanisms of flow in naturally and experimentally deformed peridotites. *Am. J. Sci.* **273**, 853–876.

Nicolas, A. & Poirier, J. P. 1976. *Crystalline Plasticity and Solid State Flow in Metamorphic Rocks.* J. Wiley and Sons, London.

Oertel, G. 1970. Deformation of a slaty, lapillar tuff in the Lake District, England. *Bull. geol. Soc. Am.* **81**, 1173–1188.

Olsen, T. S. & Kohlstedt, D. L. 1985. Natural deformation and recrystallization of some intermediate plagioclase feldspar. *Tectonophysics* **111**, 107–131.

Peselnick, L., Nicolas, A. & Stevenson, P. R. 1974. Velocity anisotropy in a mantle peridotite from the Ivrea zone: application to the upper mantle anisotropy. *J. geophys. Res.* **79**, 1175–1182.

Prinzhofer, A. & Nicolas, A. 1980. The Bogata Peninsula: a possible oceanic transform fault. *J. Geology* **88**, 387–398.

Ronov, A. B. & Yowoshervsky, A. A., 1969. Chemical composition of the earth's crust. In: *The Earth's Crust and Upper Mantle* (edited by Hart, P. J.). *Am. Geophys. Un. Geophys. Monogr.* **13**, 37–57.

Rooney, T. P. & Riecker, R. E. 1969. Experimental deformation of hornblende and amphibole. *EOS, Trans. Am. geophys. Un.* **50**, 322.

Rooney, T. P. & Riecker, R. E. 1973. Constant strain-rate deformation in amphibole minerals. Environ. Res. Pap. 430. AFCRL-TR-0045.

Rooney, T. P., Riecker, R. E. & Gavasci, A. T. 1975. Hornblende deformation features. *Geology* **3**, 364–366.

Ross, J. V. & Nielsen, K. C. 1978. High-temperature flow of wet polycrystalline enstatite. *Tectonophysics* **44**, 233–261.

Rousell, D. H. 1981. Fabric and origin of gneissic layers in anorthositic rocks of the St. Charles sill, Ontario. *Can. J. Earth Sci.* **18**, 1681–1693.

Sandmeier, K. J. & Wenzel, F. 1986. Synthetic seisograms for a complex crustal model. *Geophys. Res. Lett.* **13**, 22–25.

Schmid, S. M., Casey, M. & Starkey, J. 1981. An illustration of the advantage of a complete texture analysis described by the orientation distribution function (ODF) using quartz pole figures data. *Tectonophysics* **78**, 101–117.

Schmid, S. M. & Casey, M. 1986. Complete fabric analysis of some commonly observed quartz *c*-axis patterns. *Am. Geophys. Un. Geophys. Monogr.* **36**, 263–286.

Schwerdtner, W. M. 1964. Preferred orientation of hornblende in a banded gneiss. *Am. J. Sci.* **262**, 1212–1229.

Shelley, D. 1977. Plagioclase preferred orientation in the Haast schist, New Zealand. *J. Geol.* **85**, 635–544.

Sibson, R. H. 1979. Fault rocks and fault mechanisms. *J. geol. Soc. Lond.* **133**, 191–213.

Tullis, T. E. 1976. Experiments on the origin of slaty cleavage and schistosity. *Bull. geol. Soc. Am.* **87**, 745–753.

Tullis, J. A., Christie, J. M. & Griggs, D. T. 1973. Microstructure and preferred orientations of experimentally deformed quartzites. *Bull. geol. Soc. Am.* **84**, 297–314.

Van Houtten, P. & Wagner, F. 1985. Development of textures by slip

and twinning, In: *Preferred Orientation in Deformed Metals and Rocks* (edited by Wenk, H.-R.). Academic Press, Orlando.

Van der Molen, I. & Paterson, M. S. 1979. Experimental deformation of partially melted granite. *Contr. Miner. Petrol.* **70**, 299–318.

Van Roemund, H. L. N. 1983. Petrofabrics and microstructures of omphacites in a high temperature eclogite from the Swedish Caledonides. *Bull. Minéral.* **106**, 709–713.

Van Roemund, H. L. N. & Boland, J. N. 1981. The dislocation substructures of naturally deformed omphacites. *Tectonophysics* **78**, 403–418.

Wagner, F., Wenk, H.-R., Kern, H., Van Houtte, P. & Esling, C. 1982. Development of preferred orientation in plane strain deformed limestone: experiment and theory. *Contr. Miner. Petrol.* **80**, 132–139.

Wenk, H.-R. (editor) 1985. Carbonates. In: *Preferred Orientation in Deformed Metals and Rocks.* Academic Press, Orlando.

Wenk, H.-R., Bunge, H. J., Jansen, E. & Pannetier, J. 1986. Preferred orientation of plagioclase — neutron diffraction and U-stage data. *Tectonophysics* **126**, 271–284.

Wenk, H.-R., Takeshita, T., Bechler, E., Erskine, B. G. & Matthies, S. 1987. Pure shear and simple shear calcite textures. Comparison of experimental, theoretical and natural data. *J. Struct. Geol.* **9**, 731–745.

Willis, D. 1977. A kinematic model of preferred orientation. *Bull. geol. Soc. Am.* **88**, 883–894.